ARCHIVES OF MECHANICS
Arch. Mech. **78** (2), 79–105, 2026, https://doi.org/10.24423/aom.4843

Dispersion characteristics of shear horizontal waves in piezoelectric nanoplates: a nonlocal strain gradient theory incorporating surface effects

X. H. CHEN[1)], X. M. ZHANG[1,2)], H. M. ZHOU[1,2,*)]

[1)] *School of Mechanical and Power Engineering, Henan Polytechnic University, Jiaozuo, 454003, China*

[2)] *Mechanical Monitoring and Fault Diagnosis Research Institute, Henan Polytechnic University, Jiaozuo, 454003, China,*
e-mail[*)]: zhm_1979@163.com (corresponding author)

This paper investigates the propagation of shear horizontal (SH) waves in piezoelectric nanoplates by coupling the Gurtin–Murdoch surface model with the nonlocal strain gradient theory. The Legendre polynomial expansion method with analytical integration is developed, which reformulates the complex acoustic wave partial differential equation (PDE) solution problem into a standard generalized eigenvalue problem, thereby obtaining its dispersion relation. In contrast to conventional polynomial techniques, this approach obviates the necessity of redundant integration, thereby facilitating the derivation of comprehensive solutions over the full frequency spectrum. The validity of the proposed method is verified by calculating the phase velocities of SH waves in a piezoelectric nanoplate without surface and strain gradient effects and comparing the results with literature data. The convergence and computational efficiency of the method are also demonstrated. Results indicate that the stiffness softening dominated by the surface effect and the hardening induced by the strain gradient effect form a competitive mechanical response. The surface effect increases wave velocity, while the nonlocal strain gradient effect decreases it. This interplay is frequency-dependent, with the surface effect dominating at low frequencies and the nonlocal strain gradient effect becoming dominant at higher frequencies. These findings offer valuable insights for the design of smart nano-devices.

Key words: piezoelectric nanoplate, SH wave, Legendre polynomial expansion method, surface effect, nonlocal effect, strain gradient effect.

1. Introduction

Piezoelectric materials are key functional components in modern intelligent systems like micro-electromechanical systems (MEMS) and energy harvesters, owing to their excellent electromechanical coupling properties [1]. As device dimensions shrink to the nanoscale, their performance is increasingly governed by wave propagation characteristics, which are significantly influenced by size effects not captured by a classical continuum theory [2–4]. To address this, various non-classical theories, such as nonlocal theory [5, 6], surface elasticity [7, 8], and strain gradient theory [9, 10], have been developed to capture these scale-dependent phenomena.

These theories have significantly advanced the study of wave propagation in nanostructures. Zhou *et al.* [11] developed a model for axisymmetric elastic waves in piezoelectric nano-shells by integrating a surface piezoelectricity theory with the first-order shear deformation principle. Similarly, Seema and Singhal [12, 13] focused on the SH waves in piezoelectric nanostructures and surface acoustic wave (SAW) sensors, with a particular emphasis on the impact of surface effects. Zhang *et al.* [14] analyzed the characteristics of SH and Rayleigh waves in piezoelectric nanofilms deposited on elastic substrates, investigating the role of surface parameters. Employing the surface piezoelectricity theory and the linear spring model, Wang *et al.* [15] explored the influence of surface effects and interfacial imperfection on the characteristics of SH waves within a layered orthotropic piezoelectric semi-space. Relying solely on a single mechanism provides an inadequate and incomplete representation of the scale-dependent phenomena exhibited by nanostructures. Combined surface and nonlocal effects, Maji *et al.* [16] studied the Lamb wave propagation in piezoelectric-piezomagnetic structures, and discussed the individual and combined impacts of surface elastic constants, nonlocal parameters, and structural thickness on the dispersion. Dhua *et al.* [17] developed a model for the SH wave propagation in piezoelectric-piezomagnetic bilayers with imperfect interfacial bonding. Their findings demonstrated that the combined influence of the nonlocal scale and surface piezoelectric coupling is more significant than their individual effect. More recently, Wang *et al.* [18], who modeled wave propagation in functionally graded piezoelectric sandwich nanoplates by integrating the surface piezoelectricity theory with the nonlocal strain gradient theory. By incorporating the strain gradient as an internal variable into the constitutive model, the nonlocal strain gradient theory is able to describe the "stiffening effect" induced by strain inhomogeneity [19]. This enables the theory to predict the mechanical behavior of nanostructures with higher accuracy and reliability. Although the wave characteristics in piezoelectric nanostructures have been extensively studied, the majority of existing research has been confined to single or dual scale effects. Consequently, investigations into wave propagation that simultaneously account for surface, nonlocal, and strain gradient effects remain remarkably limited.

The study of wave characteristics in piezoelectric structures has consequently garnered significant academic interest. A diverse range of numerical and analytical methodologies have been developed and successfully applied to compute the dispersion curves for guided waves in such structures. These established methodologies include the global matrix method [20, 21] the spectral collocation method [22, 23], the power series function method [24, 25] the semi-analytical finite element method [26, 27], and the Legendre polynomial method [28, 29], among others The Legendre polynomial series expansion approach (LPSEA) is a powerful and versatile tool for modeling guided waves, known for its computational efficiency and numerical stability [30]. Nevertheless, the conventional LPSEA cannot directly handle the higher-order stress derivatives inherent in NSGT. To overcome this limitation, we develop a novel method, termed NSGT-LPSEA, which integrates NSGT with the LPSEA framework. By consolidating the fundamental wave governing equations with the boundary conditions and applying the linear companion matrix method, the original problem is transformed into a standard, solvable eigenvalue problem.

The primary contribution of this paper is the first application of the NSGT-LPSEA to investigate the shear horizontal (SH) wave propagation in a PZT-5H piezoelectric nanoplate, incorporating the combined effects of surface, nonlocality, and strain gradient. We systematically analyze how these multi-scale factors and the plate thickness influence the SH wave's dispersion behavior. The remainder of this paper is organized as follows: Section 2 details the problem formulation and the NSGT-LPSEA method. Section 3 presents and discusses the numerical results. Section 4 concludes the paper and suggests future research directions.

2. Problem statements with basic equations

2.1. Basic equation

Consider an orthotropic piezoelectric nanoplate that extends infinitely in the x and y directions and is finite in the z direction, with a thickness of h. Based on the Gurtin–Murdoch surface elasticity model, the plate consists of three parts: upper and lower surface layers and an intermediate core layer, as shown in Fig. 1. In the Cartesian coordinate system, the bottom surface of the plate coincides with the xy-plane, while the top and bottom surfaces are located at $z = h$ and $z = 0$, respectively. The surface can be regarded as a mathematically thin surface with zero thickness, and its mechanical equilibrium state is attributed to the interaction between the in-plane stresses on the surface and the reaction forces from the core layer. The polarization direction is along the y-axis, and the SH wave propagates along the x-axis in the xz-plane. The surfaces are free of external mechanical and electrical loads.

Unlike the classical continuum, the nonlocal strain gradient theory studies long-range interactions between particles. The stress at reference point x depends not only on the strain and electric field state at that position, but also on the strain and electric field state at other points x'. The basic equations, which

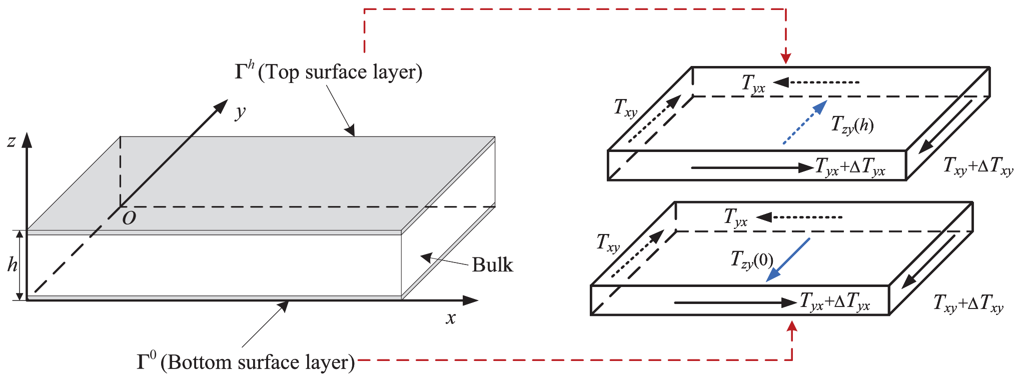

FIG. 1. Schematic diagram of a piezoelectric nanoplate.

include the effective stress equation (Eq. (2.1)) and the governing equations (Eqs. (2.2) and (2.3)), are expressed as follows [31, 32]:

$$\xi_{kl} = \sigma_{kl} - \sigma_{jkl,j}, \tag{2.1}$$

$$\xi_{kl,l} = \rho \ddot{u}_k, \tag{2.2}$$

$$D_{i,i} = 0, \tag{2.3}$$

where ξ_{kl}, σ_{kl}, and σ_{jkl} denote the effective stress tensor, classical stress tensor, nonlocal higher-order stress tensor, respectively. D_i and u_k denote the effective electric displacement tensor and displacement vector; ρ is the material density.

The relationship between the classical stress and the nonlocal higher-order stress is:

$$\sigma_{ij}(x) = \int_V \alpha(|x - x'|, e_0 a)[c_{klij}\varepsilon_{kl}(x') - e_{pij}E_p(x')]\, dV(x'), \tag{2.4}$$

$$\sigma_{mij}(x) = l_2^2 \int_V \alpha(|x - x'|, e_1 a)[c_{klij}\varepsilon_{kl,m}(x') - e_{pij}E_{p,m}(x')]\, dV(x'), \tag{2.5}$$

where $\alpha(|x - x'|, e_0 a)$ and $\alpha(|x - x'|, e_1 a)$ are the nonlocal attenuation functions, and e_0 and e_1 are relevant material parameters. a is the feature length. c_{klij} and e_{pij} represent the elastic constants and piezoelectric constants, respectively; l_2 is the strain gradient size parameter.

The generalized geometric equations are:

$$\varepsilon_{kl}(x') = \frac{1}{2}\left(\frac{\partial u_k(x')}{\partial x'_l} + \frac{\partial u_l(x')}{\partial x'_k}\right), \tag{2.6}$$

$$E_i(x') = -\frac{\partial \phi(x')}{\partial x'_i}, \tag{2.7}$$

where ε_{kl}, E_i and ϕ represent strain, electric field intensity, and electric potential.

By assuming specific forms for the non-local decay kernel functions, $\alpha(|x-x'|, e_0 a)$ and $\alpha(|x-x'|, e_1 a)$, they can be approximated by the following non-local linear differential operator [33]:

$$L_i = 1 - (e_i a)^2 \nabla^2, \quad i = 0, 1, \tag{2.8}$$

where $\nabla^2 = \partial^2/\partial x^2 + \partial^2/\partial z^2$ denotes the Laplacian operator.

Substituting Eq. (2.8) into Eqs. (2.4) and (2.5), and assuming $e_0 = e_1 = e$, yields the differential form of the general constitutive equation as follows:

$$(1 - (e_0 a)^2 \nabla^2)\sigma_{kl} = c_{klij}\varepsilon_{kl} - e_{pij}E_p, \tag{2.9}$$

$$(1 - (e_0 a)^2 \nabla^2)\sigma_{mkl} = l_2^2(c_{klij}\varepsilon_{kl,m} - e_{pij}E_{p,m}). \tag{2.10}$$

To extend the nonlocal strain gradient theory to piezoelectric nanoplates, we substitute Eqs. (2.9) and (2.10) into Eq. (2.1) while incorporating the coupling effect between the electric field and strain gradients. This yields the following constitutive equations for piezoelectric nanomaterials:

$$(1 - l_1^2 \nabla^2)\xi_{kl} = (1 - l_2^2 \nabla^2)(c_{klij}\varepsilon_{kl} - e_{pij}E_p), \tag{2.11a}$$

$$(1 - l_1^2 \nabla^2)D_i = (1 - l_2^2 \nabla^2)(e_{ikl}\varepsilon_{kl} + \kappa_{im}E_m), \tag{2.11b}$$

where κ_{im} represents the permittivity. For convenience, l_1 is used to denote $e_0 a$, representing the non-local feature parameter.

For SH waves propagating in the xz-plane, the free-harmonic solutions can be expressed as:

$$\{u_y, \phi\}\{x, z, t\} = \{U(z), V(z)\}\exp(\mathrm{i}kx - \mathrm{i}\omega t), \tag{2.12}$$

where $U(z)$ and $V(z)$ are the amplitudes of displacement and electric potential, respectively; k is the wavenumber, ω is the angular frequency, and i is the imaginary unit.

Using Voigt notation for the material parameters, the constitutive equations can be written as:

$$(1 - l_1^2 \nabla^2)\xi_{yz} = (1 - l_2^2 \nabla^2)(c_{44}\varepsilon_{yz} - e_{15}E_z), \tag{2.13a}$$

$$(1 - l_1^2 \nabla^2)\xi_{yx} = (1 - l_2^2 \nabla^2)(c_{44}\varepsilon_{yx} - e_{15}E_x), \tag{2.13b}$$

$$(1 - l_1^2 \nabla^2)D_z = (1 - l_2^2 \nabla^2)(e_{15}\varepsilon_{yz} + \kappa_{11}E_z), \tag{2.13c}$$

$$(1 - l_1^2 \nabla^2)D_x = (1 - l_2^2 \nabla^2)(e_{15}\varepsilon_{xy} + \kappa_{11}E_x). \tag{2.13d}$$

Substituting Eqs. (2.6), (2.7), (2.12) and (2.13) into Eqs. (2.2) and (2.3) yields the wave equations for the bulk that account for the nonlocal strain gradient theory:

$$\text{(2.14a)}\quad \begin{aligned} &c_{44}U'' + e_{15}V'' - l^2(c_{44}k^4U(z) + e_{15}k^4V(z)) + 2l_2^2(c_{44}k^2U''(z) \\ &\quad + e_{15}k^2V''(z)) - e_{15}k^2V(z) - c_{44}k^2U(z) - l_2^2(c_{44}U^{(4)} + e_{15}V^{(4)}) \\ &\quad = -\omega^2\rho U(z) - \rho l_1^2(k^2\omega^2U(z) - \omega^2U''(z)), \end{aligned}$$

$$\text{(2.14b)}\quad \begin{aligned} &e_{15}l_2^2k^2U''(z) - e_{15}l_2^2U^{(4)}(z) - e_{15}k^2U(z) - e_{15}l_2^2(k^4U(z) \\ &\quad - k^2U''(z)) + e_{15}U''(z) - \kappa_{11}V''(z) + k^2\kappa_{11}V(z) + l_2^2\kappa_{11}(V^{(4)}(z) \\ &\quad - k^2V''(z)) + l_2^2\kappa_{11}(k^4V(z) - k^2V''(z)) = 0. \end{aligned}$$

For the surface, the surface stress ξ_{yx}^s and surface electric displacement D_x^s are [34]:

$$\text{(2.15a)}\quad (1 - l_1^2\nabla^2)\xi_{yx}^s = (1 - l_2^2\nabla^2)(\sigma_0 + c_{44}^s u_{y,x} + e_{15}^s\phi_{,x}),$$

$$\text{(2.15b)}\quad (1 - l_1^2\nabla^2)D_x^s = (1 - l_2^2\nabla^2)(D_0 + e_{15}^s u_{y,x} - \kappa_{11}^s\phi_{,x}),$$

where c_{44}^s, e_{15}^s, and κ_{11}^s are the surface elastic, piezoelectric, and dielectric parameters, respectively, while σ_0 and D_0 represent the residual tangential stress and electric displacement induced by surface relaxation effects.

The boundary conditions for the electrically open-circuit condition, based on the surface equilibrium equations of the Gurtin–Murdoch model, are:

$$\text{(2.16)}\quad \begin{aligned} \xi_{yx,x}^s - \xi_{yz}|_{z=h} &= \rho^s\ddot{u}_y, & \xi_{yx,x}^s + \xi_{yz}|_{z=0} &= \rho^s\ddot{u}_y, \\ D_x^s - D_z|_{z=h} &= 0, & D_x^s + D_z|_{z=0} &= 0, \end{aligned}$$

where ρ^s denotes the surface density, and $\rho^s\ddot{u}_y$ denotes the inertial force in the y direction at the surface.

When analyzing the mechanical behavior of nanostructures, it is often necessary to introduce several characteristic lengths to quantify the dimensional correlation between the surface and the substrate in terms of their respective physical properties. The surface parameter can be defined as [35]:

$$\text{(2.17)}\quad c_{44}^s = f_c c_{44}, \quad e_{15}^s = f_e e_{15}, \quad \kappa_{11}^s = f_\kappa \kappa_{11}, \quad \rho^s = f_\rho \rho,$$

where f_c, f_e, f_κ, and f_ρ are the characteristic lengths of surface elasticity, surface piezoelectricity, surface dielectric property, and surface density, respectively.

Substituting Eqs. (2.12), (2.13), (2.15) and (2.17) into Eq. (2.16) yields the boundary condition equations for a piezoelectric nanoplate that accounts for both surface effects and the nonlocal strain gradient theory:

$$\text{(2.18a)}\quad \begin{aligned} &l_2^2k^2(c_{44}^sU''(z) + e_{15}^sV''(z)) - l_2^2k^4(c_{44}^sU(z) + e_{15}^sV(z)) \\ &\quad - l_2^2k^2(c_{44}U'(z) + e_{15}V'(z)) - c_{44}^sk^2U(z) - e_{15}^sk^2V(z) \\ &\quad + l_2^2(c_{44}U^{(3)}(z) + e_{15}V^{(3)}(z)) - c_{44}U'(z) - e_{15}V'(z)|_{z=h} \\ &\quad = -\rho^s\omega^2U(z) - l_1^2\rho^s(k^2\omega^2U(z) - \omega^2U''(z)), \end{aligned}$$

$$\begin{aligned}
(2.18\text{b})\quad & l_2^2k^2(c_{44}^sU''(z)+e_{15}^sV''(z))-l_2^2k^4(c_{44}^sU(z)+e_{15}^sV(z))\\
&+l_2^2k^2(c_{44}U'(z)+e_{15}V'(z))-c_{44}^sk^2U(z)-e_{15}^sk^2V(z)\\
&-l_2^2(c_{44}U^{(3)}(z)+e_{15}V^{(3)}(z))+c_{44}U'(z)+e_{15}V'(z)|_{z=0}\\
&=-\rho^s\omega^2U(z)-l_1^2\rho^s(k^2\omega^2U(z)-\omega^2U''(z)),\\
(2.18\text{c})\quad & k^2\kappa_{11}^sV(z)-e_{15}^sk^2U(z)-e_{15}^sl_2^2(k^4U(z)-k^2U''(z))\\
&+l_2^2\kappa_{11}^s(k^4V(z)-k^2V''(z))-e_{15}U'(z)+e_{15}l_2^2(U^{(3)}(z)-k^2U'(z))\\
&-l_2^2\kappa_{11}(V^{(3)}(z)-k^2V'(z))+\kappa_{11}V'(z)|_{z=h}=0,\\
(2.18\text{d})\quad & k^2\kappa_{11}^sV(z)-e_{15}^sk^2U(z)-e_{15}^sl_2^2(k^4U(z)-k^2U''(z))\\
&+l_2^2\kappa_{11}^s(k^4V(z)-k^2V''(z))+e_{15}U'(z)-e_{15}l_2^2(U^{(3)}(z)-k^2U'(z))\\
&+l_2^2\kappa_{11}(V^{(3)}(z)-k^2V'(z))-\kappa_{11}V'(z)|_{z=0}=0.
\end{aligned}$$

Equation (2.18) can be simplified to several special cases by setting specific parameters to zero. Neglecting the surface effect (c_{44}^s, e_{15}^s, κ_{11}^s, and ρ^s are set to zero) retains only the nonlocal strain gradient effect. Ignoring the nonlocal effect ($l_1 = 0$) accounts for both strain gradient and surface effects. Disregarding the strain gradient effect ($l_2 = 0$) incorporates only nonlocal and surface effects. Finally, setting all parameters to zero recovers the classical boundary condition.

2.2. Problem solving

To solve Eqs. (2.14) and (2.18), $U(z)$ and $V(z)$ are expanded into series of Legendre polynomials:

$$(2.19)\qquad U(z)=\sum_{m=0}^{\infty}p_m^{(1)}Q_m(z),\qquad V(z)=\sum_{m=0}^{\infty}p_m^{(2)}Q_m(z),$$

where $p_m^{(\alpha)}$ ($\alpha = 1, 2$) represents the undetermined coefficients of the Legendre polynomial, and

$$Q_m(z)=\sqrt{\frac{2m+1}{h}}P_m\left(\frac{2z-h}{h}\right),$$

where P_m denotes the m-th order Legendre polynomial. The polynomial converges for a finite value M of m, such that all higher-order terms can be neglected.

By substituting Eq. (2.19) into Eq. (2.14) and then multiplying on the left by $Q_l(z)$ ($l = 0, 1, \ldots, M-2$), we can integrate over $z \in [0, h]$. The orthogonality of the Legendre polynomials therefore allows us to simplify the expression, resulting in:

$$k^4 \begin{bmatrix} A_{11}^{l,m} & A_{12}^{l,m} \\ A_{21}^{l,m} & A_{22}^{l,m} \end{bmatrix} \begin{bmatrix} p_m^{(1)} \\ p_m^{(2)} \end{bmatrix} + k^2 \begin{bmatrix} B_{11}^{l,m} & B_{12}^{l,m} \\ B_{21}^{l,m} & B_{22}^{l,m} \end{bmatrix} \begin{bmatrix} p_m^{(1)} \\ p_m^{(2)} \end{bmatrix} + \begin{bmatrix} C_{11}^{l,m} & C_{12}^{l,m} \\ C_{21}^{l,m} & C_{22}^{l,m} \end{bmatrix} \begin{bmatrix} p_m^{(1)} \\ p_m^{(2)} \end{bmatrix} = k^2 \begin{bmatrix} D_{11}^{l,m} & 0 \\ 0 & 0 \end{bmatrix} \begin{bmatrix} p_m^{(1)} \\ p_m^{(2)} \end{bmatrix} + \begin{bmatrix} E_{11}^{l,m} & 0 \\ 0 & 0 \end{bmatrix} \begin{bmatrix} p_m^{(1)} \\ p_m^{(2)} \end{bmatrix}. \tag{2.20}$$

It is concisely written as:

$$k^4 \mathbf{Ap} + k^2 \mathbf{Bp} + \mathbf{Cp} = 0, \tag{2.21}$$

where

$$\mathbf{A} = \begin{bmatrix} A_{11}^{l,m} & A_{12}^{l,m} \\ A_{21}^{l,m} & A_{22}^{l,m} \end{bmatrix}, \qquad \mathbf{B} = \begin{bmatrix} B_{11}^{l,m} - D_{11}^{l,m} & B_{12}^{l,m} \\ B_{21}^{l,m} & B_{22}^{l,m} \end{bmatrix},$$

$$\mathbf{C} = \begin{bmatrix} C_{11}^{l,m} - E_{11}^{l,m} & C_{12}^{l,m} \\ C_{21}^{l,m} & C_{22}^{l,m} \end{bmatrix}, \quad \mathbf{p} = \begin{bmatrix} p_m^{(1)} \\ p_m^{(2)} \end{bmatrix};$$

m takes values $0, 1, 2, \ldots, M$. $\mathbf{A}$, $\mathbf{B}$, and $\mathbf{C}$ are $2(M-1) \times 2(M+1)$ matrices.

A direct solution for the SH wave is not possible because the boundary conditions have not yet been incorporated. We therefore substitute Eq. (2.19) into Eq. (2.18) and combine the resulting equations with Eq. (2.21). Applying the Linear Companion Matrix Method to this system yields:

$$\begin{bmatrix} \mathbf{O} & \mathbf{I} \\ \mathbf{D} & \mathbf{E} \end{bmatrix} \begin{bmatrix} \mathbf{p} \\ \mathbf{q} \end{bmatrix} = k^2 \begin{bmatrix} \mathbf{p} \\ \mathbf{q} \end{bmatrix}, \tag{2.22}$$

where $\mathbf{O}$ and $\mathbf{I}$ are the zero matrix and the identity matrix, respectively, $\mathbf{q} = k^2 \mathbf{p}$:

$$\mathbf{D} = -\begin{bmatrix} \mathbf{A} \\ \mathbf{F} \end{bmatrix}^{-1} \cdot \begin{bmatrix} \mathbf{C} \\ \mathbf{H} \end{bmatrix}, \quad \mathbf{E} = -\begin{bmatrix} \mathbf{A} \\ \mathbf{F} \end{bmatrix}^{-1} \cdot \begin{bmatrix} \mathbf{B} \\ \mathbf{G} \end{bmatrix},$$

are all $2(M+1)$ square matrices. $\mathbf{F}$, $\mathbf{G}$, $\mathbf{H}$ are the corresponding matrices at the boundary. The non-zero elements in $\mathbf{A}$, $\mathbf{B}$, $\mathbf{C}$, $\mathbf{F}$, $\mathbf{G}$, and $\mathbf{H}$ are given in Appendix.

The problem is thus reduced to a standard generalized eigenvalue problem, where the eigenvalue is k^2 and the eigenvector represents the physical field distribution. Solving for the wavenumber k at a given ω yields the $k\omega$ spectrum.

Equation (2.22) consists of three distinct integral terms, as follows:

$$G_i = \int_{-1}^{1} P_j(z) \frac{d^{(i-1)}}{dz^{(i-1)}} P_m(z)\, dz, \qquad (i = 1, 3, 5). \tag{2.23}$$

By leveraging the orthogonality and recursiveness of Legendre polynomials, the following expression is obtained:

$$G_i = \begin{cases} \sum_{v=0}^{\lfloor m/2 \rfloor} (-1)^v \dfrac{(2m-2v)!}{2^m \nu!(m-\nu)!(m-2v-i+1)!} \dfrac{2^{n+1}(n+2p)!(n+p)!}{p!(2n+2p+1)!}, & \\ \qquad m-i+1 \geq n,\ m-n-i+1 = \text{even}, & \\ \qquad m-2v-i+1 = n+2p,\ i = 1,3,5, & \\ 0, \quad \text{else}. \end{cases} \tag{2.24}$$

Conventional Legendre polynomial methods [36, 37] enforce boundary conditions using rectangular window functions, converting the governing wave equation into an eigenvalue problem via orthogonality-based integration. However, this approach is computationally inefficient due to extensive numerical integration and unsuitable for non-local nanostructures with higher-order stress derivatives. In contrast, our proposed methodology directly incorporates independent boundary conditions—including surface effects and non-local strain gradients—into the governing bulk wave equation. This unified formulation is then recast as a standard eigenvalue problem and solved with an analytically integrated Legendre polynomial technique. Consequently, this framework provides a robust and novel approach for guided wave problems, demonstrating universal applicability to both non-local nanostructures and classical macroscopic systems.

3. Numerical results and discussion

3.1. The validation of the method

Currently, no existing analytical solutions are available for SH waves in piezoelectric nanoplates that simultaneously incorporate surface effects, non-local effects, and strain gradient effects due to the complexity of the model. Therefore, we verify the present method by comparing the frequency spectrum of SH waves in a PZT-5H piezoelectric nanoplate with results obtained from the finite element software COMSOL. The computational parameters are set as follows: $h = 3$ nm, $l_1 = 0.5$ nm, $l_2 = 0$ nm, and $f_c = f_e = f_\kappa = f_\rho = 0.1$ nm. The material parameters are taken from [34]: $c_{11} = 126\times10^9$ N/m^2, $c_{33} = 117\times10^9$ N/m^2, $c_{13} = 83.9\times10^9$ N/m^2, $c_{55} = 23\times10^9$ N/m^2; $e_{31} = -6.5$ C/m^2, $e_{33} = 23.3$ C/m^2, $e_{15} = 17$ C/m^2; $\kappa_{11} = 15.05\times10^{-9}$ C^2/Nm^2, $\kappa_{33} = 13.02\times10^{-9}$ C^2/Nm^2, $\rho = 7500$ kg/m^3.

In the COMSOL finite element model, only the SH wave displacement component is retained, and a one-dimensional model along the thickness direction is established based on the weak-form partial differential equation (PDE). To address the infinite propagation characteristic in the horizontal direction, the wavenumber term is analytically introduced into the weak-form equation through dimensionality reduction; meanwhile, the surface effects and surface non-local corrections are implemented via weak contribution (boundary integral) terms on the top and bottom surfaces. The model is discretized into 480 one-dimensional elements along the thickness direction to ensure the computational accuracy of higher-order modes. In the present calculation, $M = 12$. As shown in Fig. 2, the excellent agreement between the finite element method (FEM) results and those of the present method validates the proposed approach.

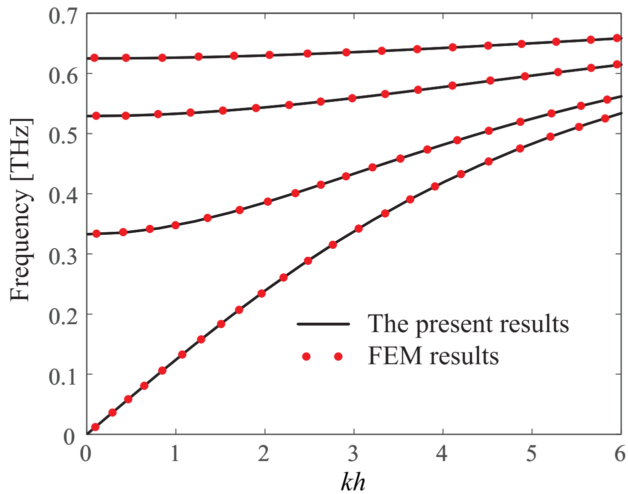

FIG. 2. Comparison of the FEM results with the present results for the frequency spectrum of SH waves in a PZT-5H piezoelectric nanoplate.

3.2. Method convergence analysis and computational efficiency

This section analyzes the convergence and computational efficiency of the NSGT-LPSEA method. As detailed in Section 3.1 and illustrated in Fig. 3, the phase velocity dispersion curves for the first eight SH wave modes are calculated for various M values. The dimensionless frequency $\Omega = \omega h/c_{sh}$ and the dimensionless wavenumber kh are used. The dimensionless phase velocity is calculated by $C_p = \omega/k/c_{sh}$, where $c_{sh} = \sqrt{(c_{44} + e_{15}^2/\kappa_{11})/\rho}$ is the shear wave velocity. The results show that for $M = 12$, the first six modes converge perfectly, whereas significant deviations appear from the seventh mode onward. The number of converged modes increases with M: at $M = 13$, the seventh mode is nearly converged, and at $M = 14$, it achieves full convergence. This pattern suggests that the first $M/2$ modes can be reliably converged, confirm-

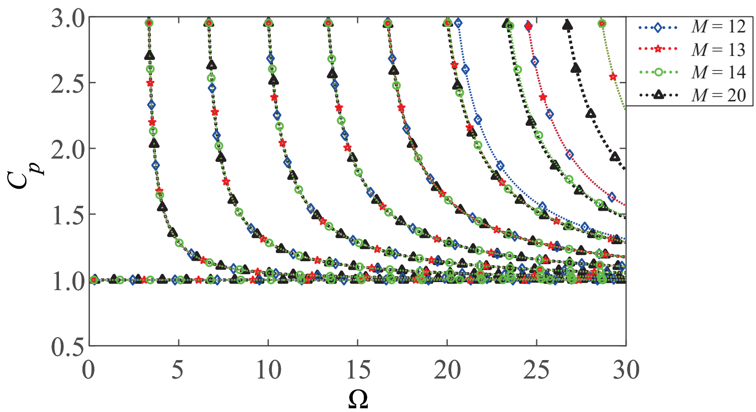

Fig. 3. Dispersion curves of the shear wave phase velocity for PZT-5H piezoelectric nanoplates at different M values.

ing the method's excellent convergence properties. $M = 20$ is selected for all subsequent calculations in this study.

To assess the computational efficiency of the proposed method, it is compared against a traditional numerical integration method documented in [38]. At a fixed frequency of $\Omega = 3$, the CPU time required for eigenvalue solution is measured for both methods across different M values. For clarity, t_1 and t_2 denote the integration and total times for our analytical method, respectively, whereas T_1 and T_2 are the corresponding times for the numerical method. All experiments are carried out on a single PC featuring an Intel® Core™ i5-14600KF CPU (3.5 GHz) and 32 GB RAM. The results are presented in Table 1.

Table 1. Computation time for two methods at different M values.

M	10	11	12	13	15	20
t_1 [s]	0.082	0.099	0.113	0.121	0.154	0.296
t_2 [s]	0.093	0.116	0.123	0.142	0.169	0.311
T_1 [s]	5.343	7.033	9.180	11.725	18.846	47.986
T_2 [s]	5.359	7.048	9.195	11.745	18.863	48.011

The computational cost of the numerical method rises sharply with increasing M. When M increases from 10 to 20, its total time (T_2) grows from 5.359 s to 48.011 s. Further analysis shows that the integration process is the main bottleneck; for instance, at $M = 15$, the integration time ($T_1 = 18.846$ s) constitutes 99.9% of the total time ($T_2 = 18.863$ s).

By contrast, the proposed NSGT-LPSEA method avoids this bottleneck through analytical integration, leading to a remarkable enhancement in computational efficiency. For $M = 10$, the total time t_2 is just 0.093 s, representing a 98.26% reduction in computation time compared to the numerical counterpart. At $M = 20$, t_2 remains low at only 0.311 s, and the performance gap expands to a 99.35% speed advantage. Clearly, the superiority of our method becomes increasingly significant as M grows.

3.3. Influence of surface and nonlocal strain gradient effects on SH wave

This section systematically investigates the influence of surface effects (SE) and nonlocal strain gradient effects (NSGE) on the SH waves in a PZT-5H nanoplate. We begin by examining the individual contributions of each mechanism, followed by an analysis of their coupled effects and the critical role of plate thickness.

3.3.1. Isolated influence of surface effects. To isolate the impact of surface effects, we compare the spectra and phase velocity dispersion curves of a classical PZT-5H nanoplate with those incorporating SE, as shown in Fig. 4. The parameters are set as $h = 4$ nm, $l_1 = l_2 = 0$, $f_c = f_e = 2$ nm, and $f_\kappa = f_\rho = 1$ nm, with other properties from Section 3.1. As depicted in Fig. 4, the inclusion of SE fundamentally alters the SH wave propagation by introducing a surface stiffening effect, which adds a restoring force at the nanoplate boundaries. This leads to significant, mode-dependent changes in phase velocity compared to the classical case.

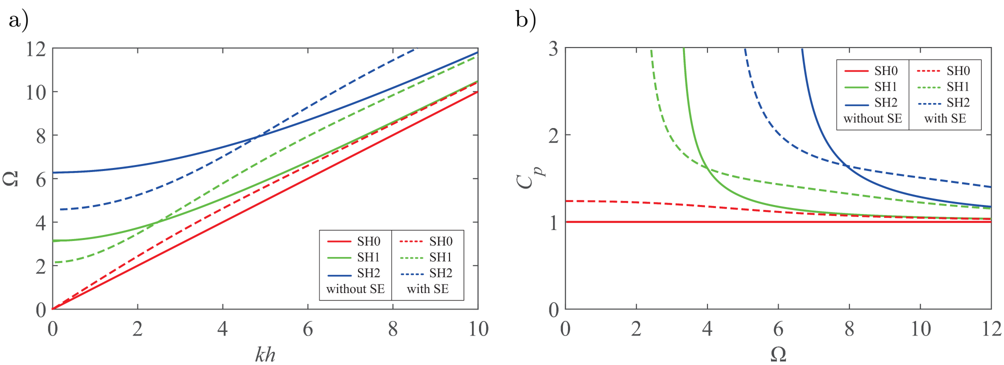

FIG. 4. Spectra and phase velocity dispersion curves of the first three modes; a) spectra, b) phase velocity dispersion curves.

For the fundamental SH0 mode, SE introduces dispersion and generally enhances the phase velocity. However, this enhancement weakens with increasing frequency, causing the velocity curve to asymptotically approach the classical wave speed c_{sh}. The physical origin of this behavior is straightforward: as frequency increases, the wavelength decreases, and the wave's energy becomes progressively confined to the plate's central region, thereby diminishing its sensitivity to the surface.

The effect on higher-order modes is more nuanced. For the SH1 mode, SE reduces the phase velocity at lower frequencies (e.g., $C_p = 1.7255$ at $\Omega = 3.5$ vs. 2.24898 classically) but increases it at higher frequencies (e.g., $C_p = 1.54546$ at $\Omega = 4.5$ vs. 1.39113 classically). A similar complex trend is observed for the SH2 mode. The underlying reason is twofold, depending on the frequency regime.

At low frequencies (near the cutoff frequency), higher-order modes possess long wavelengths. Consequently, the vibrational energy is predominantly concentrated in the plate's central region, with minimal displacement at the surfaces. In this state, the surface stress subtly alters the system's equilibrium, requiring more energy to sustain the vibrational mode. This manifests macroscopically as a reduction in the plate's effective stiffness, thereby decreasing the phase velocity. Conversely, at high frequencies (well above the cutoff frequency), the wavelength shortens. This causes the vibrational energy to distribute more uniformly across the plate's thickness and even concentrate towards the surfaces. As a result, the surface stiffening effect is "reactivated," leading to an increase in the phase velocity.

Given the high sensitivity of the SH0 and SH1 modes to surface effects, a parametric study is conducted to quantify the influence of individual surface parameters. The phase velocity dispersion curves for these modes are computed by systematically varying the surface elastic (f_c), piezoelectric (f_e), permittivity (f_κ), and density (f_ρ) parameters, with the results presented in Figs. 5–8.

Figure 5 illustrates that an increase in the surface elastic parameter f_c leads to a significant rise in phase velocity. This stiffening effect is attributed to the

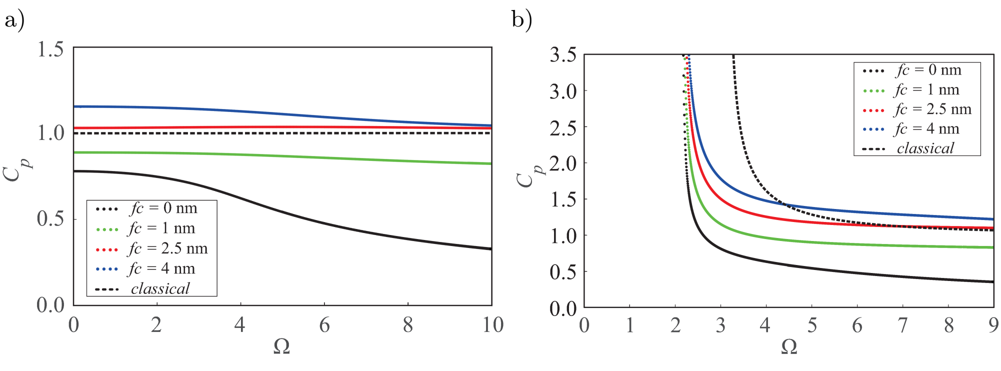

FIG. 5. Influence of f_c on phase velocity ($f_e = 0.2$ nm, $f_s = f_\rho = 1$ nm);
a) SH0 mode, b) SH1 mode.

enhancement of the system's equivalent stiffness by surface elasticity, which is directly proportional to f_c. The surface elastic parameter introduces an additional surface stress term, acting like a parallel "spring" that increases the effective stiffness, as reported in [15]. Consequently, the structure exhibits higher resistance to deformation and an increased wave velocity. For lower values of f_c (e.g., 0 nm and 1 nm), the phase velocity of the SH0 mode remains below the bulk shear wave velocity c_{sh}, with this discrepancy becoming more pronounced at higher frequencies. In contrast, for higher f_c values (2.5 nm and 4 nm), the phase velocity initially exceeds c_{sh} ($C_p > c_{sh}$) but eventually approaches c_{sh} as the frequency increases. This trend is quantitatively illustrated by the SH0 mode: at $f_c = 2.5$ nm, C_p decreases from 1.0404 ($\Omega = 2.0$) to 1.0223 ($\Omega = 9.0$); at $f_c = 4$ nm, it decreases from 1.1547 to 1.04636 over the same frequency range.

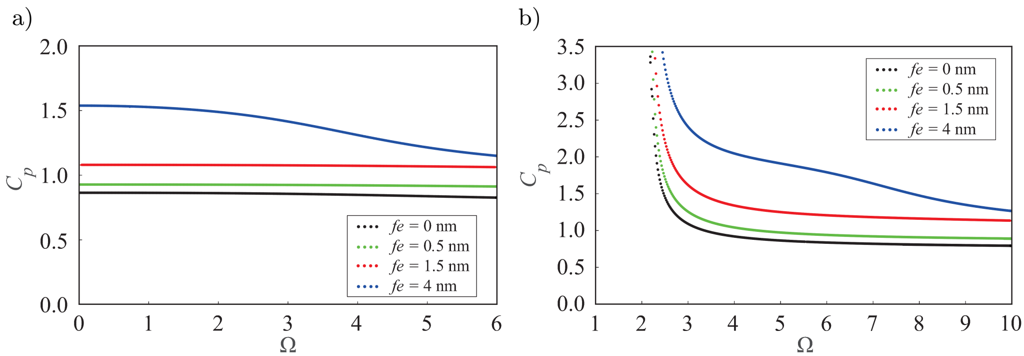

Fig. 6. Influence of f_e on phase velocity ($f_c = f_\kappa = f_\rho = 1$ nm); a) SH0 mode, b) SH1 mode.

A similar stiffening effect is observed for the surface piezoelectric parameter (f_e), as depicted in Fig 6. Conversely, Figs. 7 and 8 demonstrate that surface permittivity (f_κ) and surface density (f_ρ) both reduce the phase velocity, with a continuous decrease observed as these parameters increase. Surface density directly contributes to the overall kinetic energy of the system. Increasing the surface density is equivalent to attaching an additional mass layer to the structural surface, which raises the effective mass per unit length/area of the structure. The increase in the surface permittivity implies that the surface layer can store more electrostatic energy under the same electric field. The increase in electrostatic energy weakens a portion of the elastic potential energy, thereby reducing the effective stiffness of the system. A comparative analysis of the parametric influence reveals that f_ρ exerts the most significant effect on C_p, followed by f_c and f_e, whereas the impact of f_κ is comparatively minor. Furthermore, surface density markedly reduces the cut-off frequency, whereas the other three factors have almost no effect on it.

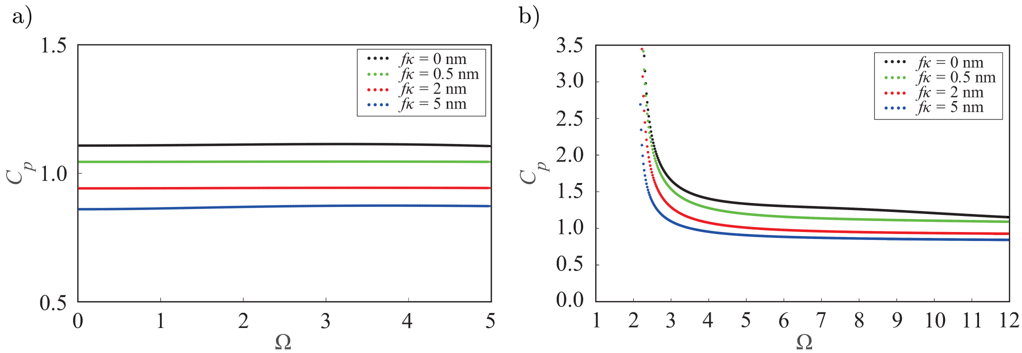

FIG. 7. Influence of f_κ on phase velocity ($f_c = f_e = f_\rho = 1$ nm); a) SH0 mode, b) SH1 mode.

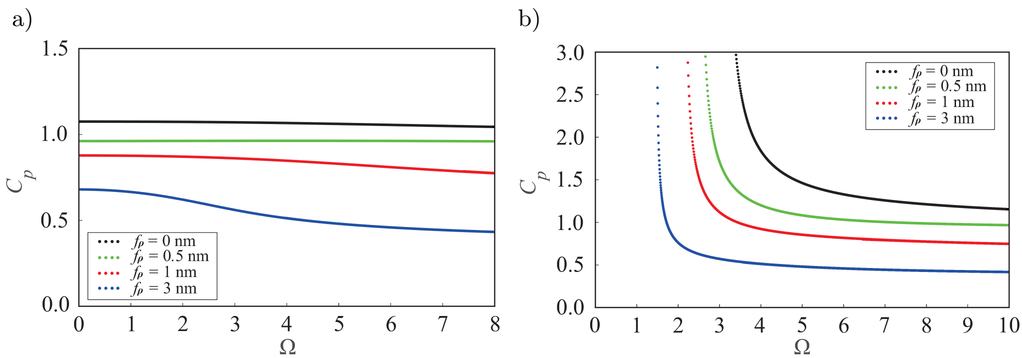

FIG. 8. Influence of f_ρ on phase velocity ($f_c = f_e = 0.5$ nm, $f_\kappa = 1$ nm);
a) SH0 mode, b) SH1 mode.

3.3.2. Isolated influence of nonlocal strain gradient effects. To illustrate the nonlocal strain gradient effect (NSGT), we first analyze the individual influences of its two constituent mechanisms: the nonlocal effect (NE) and the strain gradient effect (SGT). As shown in Fig. 9a, the NE alone ($l_2 = 0$) monotonically decreases the wave velocity, which vanishes at the escape frequency ($\Omega = 13.3247$, $C_p = 0$). This "softening" arises because at high frequencies, the wavelength becomes comparable to the nonlocal interaction range, severely diminishing the material's ability to transmit vibrations. Conversely, the SGT alone ($l_1 = 0$) increases the wave velocity above the classical value. This "stiffening" effect is also frequency-dependent, as short-wavelength waves possess large strain gradients that enhance the material's effective stiffness.

The competition between these opposing mechanisms is depicted in Figs. 9b and 9c. When $l_1 > l_2$ (Fig. 9b), the NE dominates, leading to overall softening and a wave velocity below the classical prediction. Keeping l_1 constant and increasing l_2 enhances the stiffening effect, partially counteracting the softening and causing the velocity to "rebound" towards the classical value. Conversely, when $l_1 < l_2$ (Fig. 9c), the SGT dominates, resulting in overall stiffening and a higher wave velocity. Here, increasing l_1 partially offsets the stiffening, causing the velocity to "fall back" towards the classical value. A perfect balance is achieved when $l_1 = l_2$, where the dispersion curves precisely coincide with classical theory. This indicates that the stiffness enhancement from the SGT exactly counterbalances the reduction from the NE, a physical mechanism fully consistent with the mathematical relationship in Eq. (2.11).

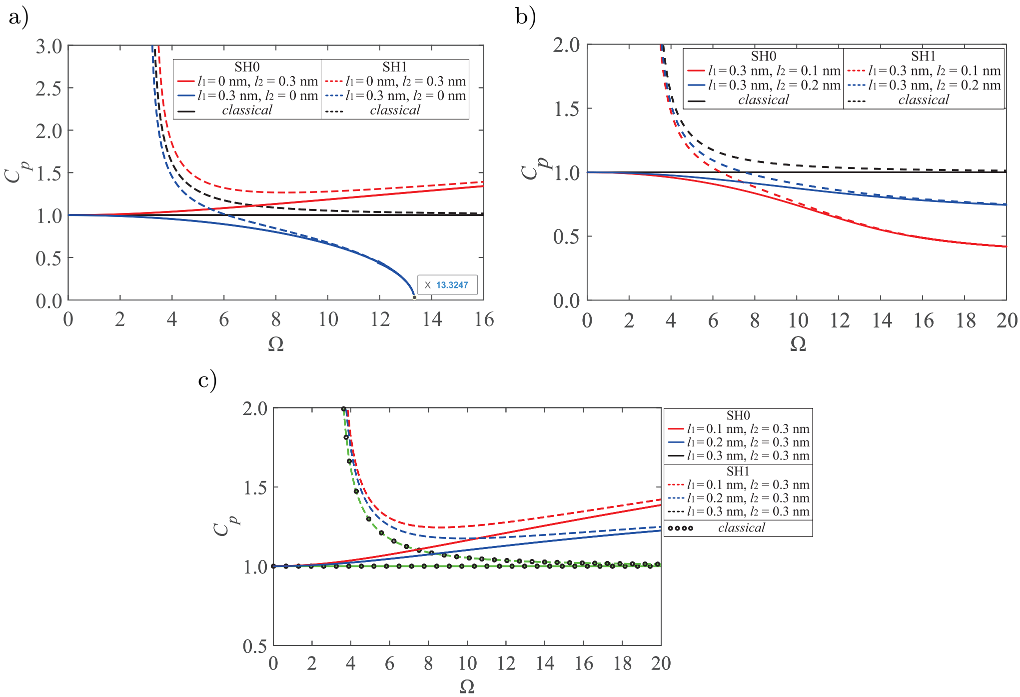

Fig. 9. Phase velocity dispersion curves of SH0 and SH1 modes for different scale parameters; a) $l_1 = 0$ or $l_2 = 0$, b) $l_1 > l_2$, c) $l_1 < l_2$.

With the underlying mechanisms established, we now investigate the overall influence of the NSGT under specific material parameters. Similarly, the influence of the NSGT is investigated by comparing the spectra and phase velocity dispersion curves of the first three SH wave modes in classical PZT-5H nanoplates against those incorporating the NSGT (Fig. 10), with material length scales $l_1 = 0.1$ nm and $l_2 = 0.2$ nm and surface effects neglected. The analysis reveals that because $l_2 > l_1$, the SGT is the dominant factor, and the NSGT generally increases the phase velocity. This enhancement is more significant at

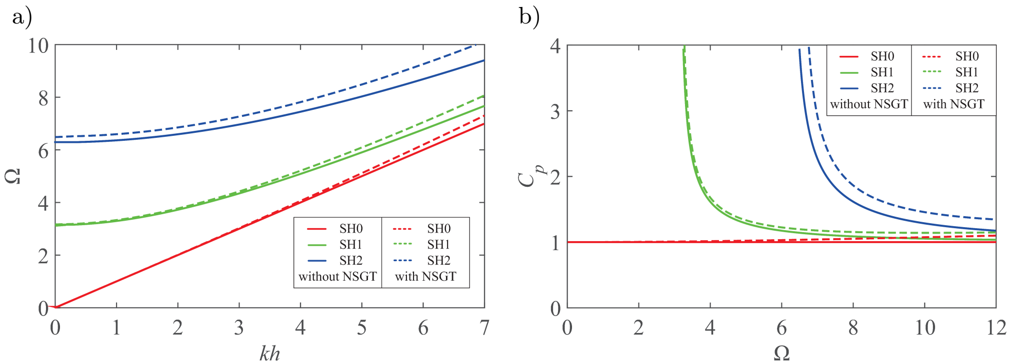

FIG. 10. Effect of NSGT on SH waves; a) spectrum, b) phase velocity dispersion curve.

higher frequencies and for higher-order modes. Regarding cutoff frequencies, the NSGT has a negligible effect on the SH1 mode but markedly increases that of the SH2 mode.

3.3.3. Coupled influence of surface and nonlocal strain gradient effects. The mutual coupling, competition, and suppression among surface effects (SE), nonlocal effects (NE), and strain gradient effects (SGT) create a complex landscape for wave propagation. A key finding is that the dominant mechanism is not fixed but can transition with frequency, leading to intricate dispersion behaviors.

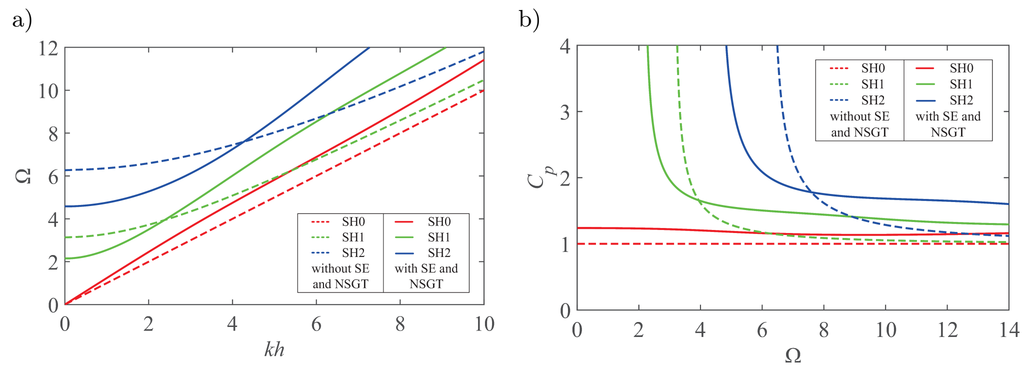

FIG. 11. Dispersion curves of SH waves in PZT-5H nanoplates considering SE and NSGT; a) frequency spectra, b) phase velocity dispersion curves.

Figure 11 presents the frequency spectra and phase velocity dispersion curves for the SH0, SH1 and SH2 modes, incorporating both SE and NSGT with parameters $f_c = f_e = 2$ nm, $f_\kappa = f_\rho = 1$ nm, $l_1 = 0.1$ nm, and $l_2 = 0.2$ nm. A comparison with Figs. 4 and 10 reveals that the combined SE-NSGT curves closely resemble those considering only SE. This similarity arises because, under these parameters, the influence of SE is significantly stronger than that of NSGT, making it the dominant factor.

To generalize, we analyze the SH0 and SH1 modes. Figure 12 compares their dispersion curves under five conditions: (1) classical; (2) SE only; (3) nonlocal (NE) only; (4) strain gradient (SGT) only; and (5) combined SE and NSGT.

For the SH0 mode (Fig. 12a), SE and NE effects have opposing influences on the phase velocity (C_p): SE increases C_p, while NE decreases it. Similarly, NE and SGT effects are opposing. When both SE and NSGT are considered, a transition in the dominant mechanism occurs. For $\Omega < 6.7$, the influence of SE is stronger than that of NSGT, causing the velocity to be higher than the classical value. For $\Omega > 8.5$, the influence of NSGT becomes dominant, with its stiffening NSGT component ($l_2 > l_1$) leading to a further increase in velocity. This behavior is consistent with the single-mechanism analysis presented earlier.

Figure 12b shows that SE significantly reduces the cutoff frequency of the SH1 mode. Similar to the SH0 mode, a transition in the dominant mechanism is observed: SE dominates at lower frequencies ($\Omega < 5.4$), while NSGT governs at higher frequencies. To quantify this interplay, we compare the phase velocities at $\Omega = 6$, a point within the NSGT-governed regime for the SH1 mode. The resulting C_p values are: NE only (1.0111), classical (1.17596), SGT only (1.3203), SE only (1.4459), and the combined model (1.5018), which yields the highest velocity.

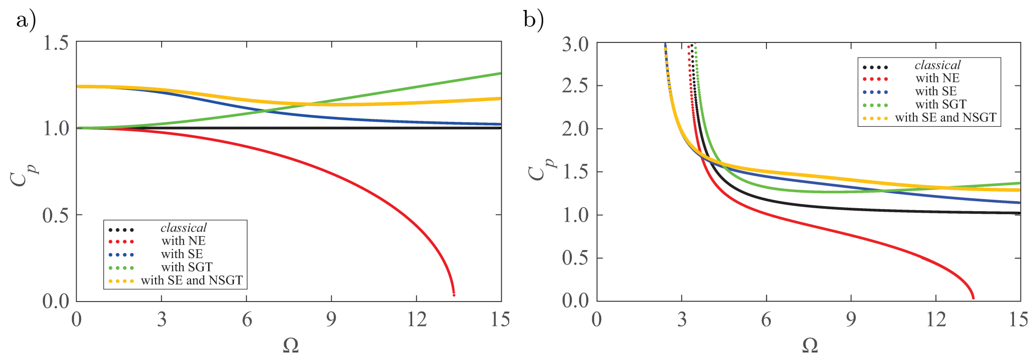

Fig. 12. Phase velocity dispersion curves of SH waves considering multiple effects; a) SH0 mode, b) SH1 mode.

3.4. The critical role of plate thickness

3.4.1. Size-dependence from surface effects. Within the classical continuum framework, SH wave characteristics are independent of plate thickness [39, 40]. This invariance is broken when surface effects (SE) are introduced. As shown in Fig. 13, SE induces significant size-dependence in the dispersion behavior of SH waves in a piezoelectric nanoplate (with $f_c = f_e = 2$ nm, $f_\kappa = f_\rho = 1$ nm).

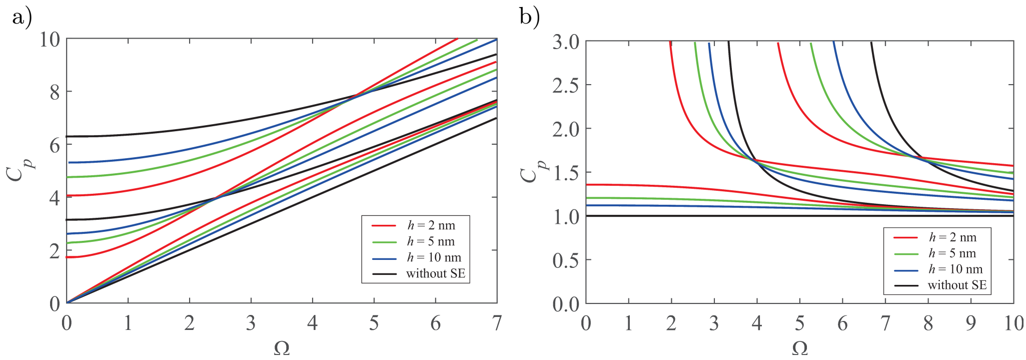

FIG. 13. Influence of h on the first three modes considering only surface effects; a) frequency spectra, b) phase velocity curves.

The physical origin of this phenomenon is the disparity in material properties between the surface layer and the bulk. As the plate thickness diminishes, the relative contribution of the surface layer increases, thereby altering the nanoplate's equivalent material parameters.

This size-dependence is markedly mode-dependent. For the fundamental SH0 mode, the phase velocity (C_p) decreases as the plate thickness increases, an effect most pronounced at low frequencies. For the higher-order SH1 and SH2 modes, the trend is more complex: at low frequencies, C_p increases with h, whereas at high frequencies, it decreases. Furthermore, the cutoff frequency is also highly sensitive to thickness, increasing concurrently with h.

3.4.2. Size-dependence from nonlocal strain gradient effects. Similarly, the nonlocal strain gradient theory (NSGT) also endows the nanoplate with pronounced size-dependent characteristics. Figure 14 illustrates the influence of plate

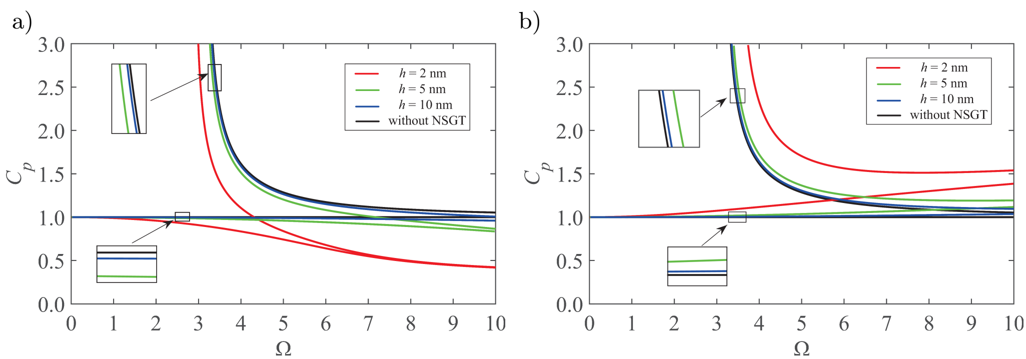

FIG. 14. Influence of h on the phase dispersion of the first two modes considering only NSGT; a) $l_1 > l_2$, b) $l_1 < l_2$.

thickness on the first two SH modes for two distinct cases: Case I ($l_1 > l_2$) where nonlocal effects dominate, and Case II ($l_1 < l_2$) where strain gradient effects are predominant.

The results reveal opposing trends. When nonlocal effects dominate (Fig. 14a), the phase velocity exhibits a positive correlation with plate thickness. Conversely, when the strain gradient effect is more significant (Fig. 14b), the velocity decreases as h increases. A critical observation in both cases is the convergence of the dispersion curves towards the classical solution as h increases. This asymptotic behavior confirms that the NSGT model reduces to its classical counterpart for sufficiently thick plates, where the nanoscale effects become negligible.

3.4.3. Competition and critical thickness. To investigate the interplay between SE and NSGT, Fig. 15 presents the relationship between phase velocity and plate thickness at a fixed dimensionless frequency ($\Omega = 5$) for five cases: classical, SE-only, NSGT-only, and their combination. The parameters are set as $f_c = f_e = 2$ nm, $f_\kappa = f_\rho = 1$ nm, $l_1 = 0.3$ nm, and $l_2 = 0.2$ nm. A dimensionless thickness $\bar{h} = h/h^*$ ($h^* = 1$ m) is introduced, and $H = \lg(\bar{h})$ is defined.

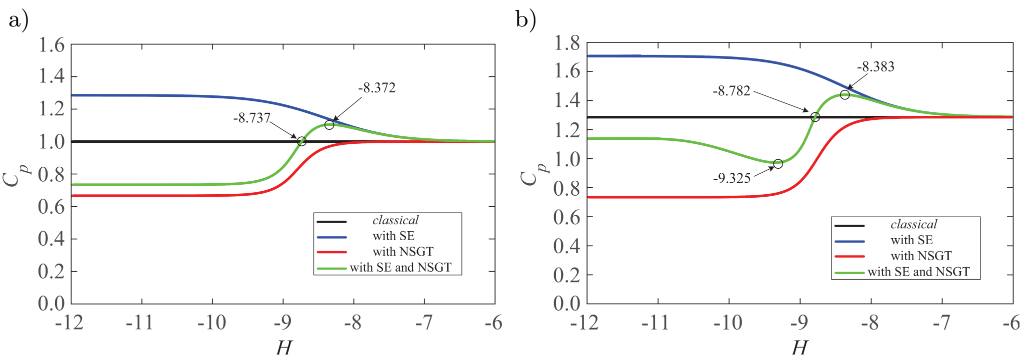

FIG. 15. Phase velocity versus plate thickness; a) SH0 mode, b) SH1 mode.

As expected, the classical model shows no thickness dependence. At the nanoscale, however, SE and NSGT introduce strong and antagonistic size-dependence: SE enhances the wave velocity, while NSGT attenuates it. The competition between these two effects results in a critical plate thickness (H_c). Below this critical value ($H_c \approx -8.737$ for SH0 and $H_c \approx -8.782$ for SH1), the attenuating NSGT effect prevails, and the wave velocity is lower than the classical value. Above this threshold, the enhancing SE effect dominates, causing the velocity to exceed the classical value.

This trend is non-monotonic. After surpassing the critical thickness, the phase velocity reaches a peak (at $H \approx -8.372$ for SH0 and $H \approx -8.383$ for SH1) before declining and asymptotically converging to the classical limit for sufficiently thick plates (e.g., $H > -6.476$). Moreover, the response of different modes below the critical thickness varies, with the SH0 mode's velocity increasing with h, while the SH1 mode exhibits a more complex, non-monotonic trend. This highlights the heightened sensitivity of higher-order modes to dimensional changes.

4. Conclusions

This study investigates SH waves in piezoelectric nanoplates by incorporating surface elasticity into the nonlocal strain gradient theory. Using the refined Legendre polynomial method, we derive the dispersion relations and perform a comprehensive parametric study. The key conclusions are summarized as follows:

(1) The efficient Legendre polynomial method with analytical integration is developed to solve the governing equations. This approach overcomes the limitations of conventional polynomial methods in handling complex electromechanical boundary conditions.

(2) Surface effects fundamentally alter the SH wave propagation in a mode-dependent manner via competing mechanisms. They stiffen the fundamental SH0 mode (increasing phase velocity) and lower cutoff frequencies of higher modes. This stems from a competition: surface elasticity and piezoelectricity increase wave velocity, whereas surface permittivity and density decrease it.

(3) Within the NSGT, material stiffness is governed by competing microstructural mechanisms: nonlocal "softening" versus strain-gradient "stiffening." The net effect on wave velocity depends on the balance between their characteristic length scales, enabling wave propagation engineering by tuning intrinsic parameters.

(4) When both surface and NSGT effects are present, dominance depends on frequency. Surface effects prevail at low frequencies, but as frequency increases, strain-gradient (SGT) stiffening takes over. This dynamic shift produces intricate dispersion curves.

(5) Competing surface and NSGT effects yield a critical thickness, H_c. Below H_c, NSGT softening dominates, dropping wave velocity below classical limits; above H_c, surface stiffening prevails, raising it above. This non-monotonic trend peaking near H_c enables precise size-dependent wave control in nanodevices.

The findings of this study pave the way for designing advanced nano-piezoelectric devices with tunable wave properties. Future research could extend this framework to more complex scenarios, such as incorporating thermo-mechanical coupling, exploring multi-layered structures, and analyzing waves in cylindrical or sector-shaped structures.

Appendix

$$A_{11}^{l,m} = -c_{44} l_2^2 \int\limits_0^h Q_l(z) Q_m(z)\, dz,$$

$$A_{12}^{l,m} = -e_{15} l_2^2 \int\limits_0^h Q_l(z) Q_m(z)\, dz,$$

$$A_{21}^{l,m} = -e_{15} l_2^2 \int\limits_0^h Q_l(z) Q_m(z)\, dz,$$

$$A_{22}^{l,m} = -\kappa_{11} l_2^2 \int\limits_0^h Q_l(z) Q_m(z)\, dz,$$

$$B_{11}^{l,m} = -c_{44} \int\limits_0^h Q_l(z) Q_m(z)\, dz + 2c_{44} l_2^2 \int\limits_0^h Q_l(z) \frac{d^2}{dz^2} Q_m(z)\, dz + \omega^2 \rho l_1^2 \int\limits_0^h Q_l(z) Q_m(z)\, dz,$$

$$B_{12}^{l,m} = -e_{15} \int\limits_0^h Q_l(z) Q_m(z)\, dz + 2e_{15} l_2^2 \int\limits_0^h Q_l(z) \frac{d^2}{dz^2} Q_m(z)\, dz,$$

$$B_{21}^{l,m} = -e_{15} \int\limits_0^h Q_l(z) Q_m(z)\, dz + 2e_{15} l_2^2 \int\limits_0^h Q_l(z) \frac{d^2}{dz^2} Q_m(z)\, dz,$$

$$B_{22}^{l,m} = -\kappa_{11} \int\limits_0^h Q_l(z) Q_m(z)\, dz - 2\kappa_{11} l_2^2 \int\limits_0^h Q_l(z) \frac{d^2}{dz^2} Q_m(z)\, dz,$$

$$C_{11}^{l,m} = c_{44} \int\limits_0^h Q_l(z) \frac{d^2}{dz^2} Q_m(z)\, dz - c_{44} l_2^2 \int\limits_0^h Q_l(z) \frac{d^4}{dz^4} Q_m(z)\, dz + \omega^2 \rho \int\limits_0^h Q_l(z) Q_m(z)\, dz - \rho l_1^2 \omega^2 \int\limits_0^h Q_l(z) \frac{d^2}{dz^2} Q_m(z)\, dz,$$

$$C_{12}^{l,m} = e_{15} \int\limits_0^h Q_l(z) \frac{d^2}{dz^2} Q_m(z)\, dz - e_{15} l_2^2 \int\limits_0^h Q_l(z) \frac{d^4}{dz^4} Q_m(z)\, dz,$$

$$C_{21}^{l,m} = e_{15} \int_0^h Q_l(z) \frac{d^2}{dz^2} Q_m(z)\, dz - e_{15} l_2^2 \int_0^h Q_l(z) \frac{d^4}{dz^4} Q_m(z)\, dz,$$

$$C_{22}^{l,m} = -\kappa_{11} \int_0^h Q_l(z) \frac{d^2}{dz^2} Q_m(z)\, dz + \kappa_{11} l_2^2 \int_0^h Q_l(z) \frac{d^4}{dz^4} Q_m(z)\, dz,$$

$$F_{11}^m = -c_{44}^s l_2^2 Q_m(h), \qquad F_{12}^m = -e_{15}^s l_2^2 Q_m(h),$$

$$F_{21}^m = -e_{15}^s l_2^2 Q_m(h), \qquad F_{22}^m = -\kappa_{11}^s l_2^2 Q_m(h),$$

$$F_{31}^m = -c_{44}^s l_2^2 Q_m(0), \qquad F_{32}^m = -e_{15}^s l_2^2 Q_m(0),$$

$$F_{41}^m = -e_{15}^s l_2^2 Q_m(0), \qquad F_{42}^m = \kappa_{11}^s l_2^2 Q_m(0),$$

$$\begin{aligned} G_{11}^m = {} & -c_{44}^s Q_m(h) + c_{44}^s l_2^2 (Q_m(z))''(z \to h) \\ & + c_{44} l_2^2 (Q_m(z))'(z \to h) + \rho^s l_1^2 \omega^2 Q_m(h), \end{aligned}$$

$$G_{12}^m = -e_{15}^s Q_m(h) + e_{15}^s l_2^2 (Q_m(z))''(z \to h) + e_{15} l_2^2 (Q_m(z))'(z \to h),$$

$$G_{21}^m = -e_{15}^s Q_m(h) + e_{15}^s l_2^2 (Q_m(z))''(z \to h) - e_{15} l_2^2 (Q_m(z))'(z \to h),$$

$$G_{22}^m = \kappa_{11}^s Q_m(h) - \kappa_{11}^s l_2^2 (Q_m(z))''(z \to h) + \kappa_{11} l_2^2 (Q_m(z))'(z \to h),$$

$$\begin{aligned} G_{31}^m = {} & -c_{44}^s Q_m(0) + c_{44}^s l_2^2 (Q_m(z))''(z \to 0) \\ & - c_{44} l_2^2 (Q_m(z))'(z \to 0) + \rho^s l_1^2 \omega^2 Q_m(0), \end{aligned}$$

$$G_{32}^m = -e_{15}^s Q_m(0) + e_{15}^s l_2^2 (Q_m(z))''(z \to 0) - e_{15} l_2^2 (Q_m(z))'(z \to 0),$$

$$G_{41}^m = -e_{15}^s Q_m(0) + e_{15}^s l_2^2 (Q_m(z))''(z \to 0) + e_{15} l_2^2 (Q_m(z))'(z \to 0),$$

$$G_{42}^m = \kappa_{11}^s Q_m(0) - \kappa_{11}^s l_2^2 (Q_m(z))''(z \to 0) - \kappa_{11} l_2^2 (Q_m(z))'(z \to 0),$$

$$\begin{aligned} H_{11}^m = {} & -c_{44} (Q_m(z))'(z \to h) - c_{44} l_2^2 (Q_m(z))'''(z \to h) \\ & - \rho^s l_1^2 \omega^2 (Q_m(z))''(z \to h) + \rho^s \omega^2 Q_m(h), \end{aligned}$$

$$H_{12}^m = -e_{15} (Q_m(z))'(z \to h) - l_2^2 e_{15} (Q_m(z))'''(z \to h),$$

$$H_{21}^m = -e_{15} (Q_m(z))'(z \to h) + l_2^2 e_{15} (Q_m(z))'''(z \to h),$$

$$H_{22}^m = \kappa_{11} (Q_m(z))'(z \to h) - l_2^2 \kappa_{11} (Q_m(z))'''(z \to h),$$

$$\begin{aligned} H_{31}^m = {} & c_{44} (Q_m(z))'(z \to 0) + c_{44} l_2^2 (Q_m(z))'''(z \to 0) \\ & - \rho^s l_1^2 \omega^2 (Q_m(z))''(z \to 0) + \rho^s \omega^2 Q_m(0), \end{aligned}$$

$$H_{32}^m = e_{15} (Q_m(z))'(z \to 0) + l_2^2 e_{15} (Q_m(z))'''(z \to 0),$$

$$H_{41}^m = e_{15} (Q_m(z))'(z \to 0) - l_2^2 e_{15} (Q_m(z))'''(z \to 0),$$

$$H_{42}^m = -\kappa_{11} (Q_m(z))'(z \to 0) + l_2^2 \kappa_{11} (Q_m(z))'''(z \to 0).$$

Acknowledgments

This work was supported by the National Natural Science Foundation of China (No. 12102131), the Natural Science Foundation of Henan Province (No. 262300421842), the Henan Provincial International Science and Technology Cooperation Project (No. 252102520074) and the Fundamental Research Funds for the Universities of Henan Province (No. NSFRF2602020).

Conflict of interest

The authors declare that they have no conflict of interest to this work.

References

1. V.E. Ogbonna, A.P.I. Popoola, O.M. Popoola, *Piezoelectric ceramic materials on transducer technology for energy harvesting: A review*, Frontiers in Energy Research, **10**, 1051081, 2022.
2. M.L. Chi, S.B. Chang, H.D. Zheng, Y.L. Wang, X.Y. Qian, Y. Ma, S.J. Wu, G.M. Zhang, *Magnetic propulsion performance of a compound spiral micro-robot applied in viscoelastic environment*, Journal of the Brazilian Society of Mechanical Sciences and Engineering, **45**, 9, 468, 2023.
3. W.W. Feng, H.Y. Chen, Q.P. Zou, D. Wang, X. Luo, C. Cummins, C.Q. Zhang, S.J. Yang, Y.X. Su, *A Contactless coupled pendulum and piezoelectric wave energy harvester: Model and experiment*, Energies, **17**, 4, 876, 2024.
4. P. Phung-Van, C.H. Thai, M. Abdel-Wahab, H. Nguyen-Xuan, *Optimal design of FG sandwich nanoplates using size-dependent isogeometric analysis*, Mechanics of Materials, **142**, 103277, 2020.
5. Y.X. Zhang, X.Q. Song, *Effects of initial stress on plane waves in piezoelectric nanoplates in liquid through integral nonlocal elasticity*, Journal of the Brazilian Society of Mechanical Sciences and Engineering, **47**, 8, 372, 2025.
6. Z. Rahimi, G. Rezazadeh, W. Sumelka, X.J. Yang, *A study of critical point instability of micro and nano beams under a distributed variable-pressure force in the framework of the inhomogeneous non-linear nonlocal theory*, Archives of Mechanics, **69**, 6, 413–433, 2017.
7. W.B. Wu, H.B. Zhang, F. Jia, X. Yang, H.D. Liu, W.F. Yuan, X.Q. Feng, B. Gu, *Surface effects on frequency dispersion characteristics of Lamb waves in a nanoplate*, Thin Solid Films, **697**, 137831, 2020.
8. Z. Kong, F.W. Qiang, P.J. Wei, Q. Tang, *Surface effects on the wave propagation in composites with random dispersive parallel cylindrical nanofibers*, Archives of Mechanics, **67**, 5, 355–370, 2015.
9. S. Biswas, *The propagation of plane waves in nonlocal visco-thermoelastic porous medium based on nonlocal strain gradient theory*, Waves in Random and Complex Media, **34**, 1, 372–403, 2024.

10. X.F. Zhang, J. Meng, B.D. Gu, W. Peng, T.H. He, *Investigation on thermoelastic wave propagation of FG multilayer hybrid nanocomposite microbeam reinforced by CNTs and GPLs under nonlocal strain gradient theory and G-N theory*, ZAMM – Zeitschrift für Angewandte Mathematik und Mechanik, **105**, 1, e202400951, 2025.

11. Y.Y. Zhou, *The surface effect on axisymmetric wave propagation in piezoelectric cylindrical shells*, Advances in Mechanical Engineering, **7**, 2, 1687814014568503, 2015.

12. Seema, A. Singhal, *Investigation of surface and interface effects of piezoelectric quasicrystal different models with propagation of shear horizontal and anti-plane shear horizontal wave*, Acta Mechanica Sinica, **41**, 11, 524389, 2025.

13. Seema, A. Singhal, *Mechanics of SH and anti-plane SH waves in orthotropic piezoelectric quasicrystal with multiple surface effect*, Acta Mechanica, **236**, 1, 439–456, 2025.

14. L.L. Zhang, J. Zhao, G.Q. Nie, J.X. Liu, *Propagation of Rayleigh-type surface waves in a layered piezoelectric nanostructure with surface effects*, Applied Mathematics and Mechanics, **43**, 3, 327–340, 2022.

15. X. Wang, Q. Chen, Y. Xue, *SH waves in orthotropic piezomaterials considered surface effects*, International Journal of Mechanical Sciences, **280**, 109529, 2024.

16. A. Maji, A.S. Kumar, S. Dhua, *Effect of nonlocality and surface – interface elasticity on lamb wave propagation in piezoelectric – piezomagnetic nanoplate*, Mechanics of Advanced Materials and Structures, **33**, 1, 2450064, 2026, https://doi.org/10.1080/15376494.2025.2450064.

17. S. Dhua, S. Mondal, A. Maji, *Surface effects on wave propagation in piezoelectric–piezomagnetic loosely bonded bilayer system using nonlocal theory of elasticity*, Thin-Walled Structures, **197**, 111612, 2024.

18. J. Wang, J. Liu, B. Hu, B. Zhang, X.T. Wang, Y.X. Wang, J. Wang, *Wave propagation in functionally graded piezoelectric sandwich nanoplates based on nonlocal strain gradient theory incorporating surface effects*, Smart Materials and Structures, **34**, 1, 015026, 2025.

19. T. Gortsas, D.G. Aggelis, D. Polyzos, *The strain gradient elasticity via nonlocal considerations*, International Journal of Solids and Structures, **269**, 112177, 2023.

20. M. Dana, J. Bernard, L. Maxit, *A spectral global matrix method for modelling the response of a fluid-loaded multilayered cylindrical shell excited by an acoustic plane wave*, Journal of the Acoustical Society of America, **148**, 5, 2997–3013, 2020.

21. A.R. Nandyala, A.K. Darpe, S.P. Singh, *Effective stiffness matrix method for predicting the dispersion curves in general anisotropic composites*, Archive of Applied Mechanics, **89**, 9, 1923–1938, 2019.

22. M. Molavi-Arabshahi, J. Rashidinia, S. Tanoomand, *An efficient spectral collocation method based on the generalized Laguerre polynomials to multi-term time fractional diffusion-wave equations*, AIP Advances, **14**, 2, 025227, 2024.

23. D.A. Hammad, M.S. El-Azab, *Chebyshev–Chebyshev spectral collocation method for solving the generalized regularized long wave (GRLW) equation*, Applied Mathematics and Computation, **285**, 2, 228–240, 2016.

24. J. Zhang, X. Tian, *Laplace-residual power series method for solving fractional generalized long wave equations*, Ocean Engineering, **310**, 118693, 2024.

25. S. Liu, Z. Fu, S. Liu, Q. Zhao, *Power series expansion method and its applications to nonlinear wave equation*, Physics Letters A, **309**, 3-4, 234–239, 2003.

26. W. Ding, L. Li, H. Zhong, Y. Li, D. Bao, S. Wei, W. Wang, *A semi-analytical wavelet finite element method for wave propagation in rectangular rods*, Wave Motion, **128**, 103325, 2024.

27. C.A. Galán-Pinilla, J. E-Quiroga, D.Y. Peña-Ballesteros, C.A. Acosta-Minoli, O.A. González-Estrada, *Comparative study of dispersion curves for Lamb waves using analytical solutions and semi-analytical methods*, Applied Sciences-Basel, **13**, 3, 1706, 2023.

28. H. Qiao, X. Wang, X. Zhang, W. Ren, *Guided wave propagation in piezoelectric bars with parallelogram cross-section: An improved double orthogonal polynomial approach*, Mathematics and Computers in Simulation, **248**, 644–667, 2026.

29. J. Gao, Y. Lyu, G. Song, M. Liu, M. Zhang, C. He, Y. Lee, *Legendre orthogonal polynomial method in calculating reflection and transmission coefficients of fluid-loaded functionally gradient plates*, Wave Motion, **104**, 102754, 2021.

30. M. Behnood, A. Shokri, *A Legendre spectral element method for the family of regularized long wave equations*, Mathematics and Computers in Simulation, **201**, 239–253, 2022.

31. X. Zhang, Seema, *Propagation of SH waves in piezo-flexoelectric-layered structures with imperfect interfaces: Analytical formulation and data-driven surrogates*, International Journal of Applied Mechanics, 2026, https://doi.org/10.1142/S1758825126500420.

32. C.W. Lim, G. Zhang, J. Reddy, *A higher-order nonlocal elasticity and strain gradient theory and its applications in wave propagation*, Journal of the Mechanics and Physics of Solids, **78**, 298–313, 2015.

33. C. Li, P. Wei, X. Guo, *The spectral methods for the propagation of thermoelastic waves in multilayer cylinders based on nonlocal strain gradient elasticity*, Acta Mechanica, **237**, 2, 647–669, 2024.

34. L. Zhang, J. Liu, X. Fang, G. Nie, *Effects of surface piezoelectricity and nonlocal scale on wave propagation in piezoelectric nanoplates*, European Journal of Mechanics A – Solids, **46**, 22–29, 2014.

35. L. Zhang, J. Liu, X. Fang, G. Nie, *Surface effect on size-dependent wave propagation in nanoplates via nonlocal elasticity*, Philosophical Magazine, **94**, 18, 2009–2020, 2014.

36. L. Elmaimouni, E. Lefebvre, F.E. Ratolojanahary, Raherison, T. Gryba, J. Carlier, *Modal analysis and harmonic response of resonators: An extension of a mapped orthogonal functions technique*, Wave Motion, **48**, 1, 93–104, 2011.

37. C. He, H. Liu, Z. Liu, B. Wu, *The propagation of coupled Lamb waves in multilayered arbitrary anisotropic composite laminates*, Journal of Sound and Vibration, **332**, 26, 7243–7256, 2013.

38. C. Othmani, F. Takali, A. Njeh, *Investigating and modeling of effect of piezoelectric material parameters on shear horizontal (SH) waves propagation in PZT-5H, PMN-0.33 PT and PMN-0.29 PT plates*, Optik, **148**, 63–75, 2017.

39. D. Li, S. Li, C. Zhang, W. Chen, *Propagation characteristics of shear horizontal waves in piezoelectric semiconductor nanoplates incorporating surface effect*, International Journal of Mechanical Sciences, **247**, 108201, 2023.

40. X. Wang, P. Yu, H. Qiao, J. Yu, X. Zhang, *Formulation of SH wave characteristics in nonlocal nanoplates*, ZAMM – Zeitschrift für Angewandte Mathematik und Mechanik, **103**, 202200322, 2023.

Received December 1, 2025; revised version June 10, 2026.
Published online July 9, 2026.